J|A|C|S
ARTICLES
Published on Web 02/15/2003

Simulating the Nucleation of Water/Ethanol and Water/*n*-Nonane Mixtures: Mutual Enhancement and Two-Pathway Mechanism

Bin Chen,*,† J. Ilja Siepmann,‡ and Michael L. Klein†

Contribution from the Center for Molecular Modeling and Department of Chemistry, University of Pennsylvania, 231 S. 34th Street, Philadelphia, Pennsylvania 19104-6323, and Departments of Chemistry and of Chemical Engineering and Materials Science, University of Minnesota, 207 Pleasant Street S.E., Minneapolis, Minnesota 55455-0431

Received October 18, 2002 ; E-mail: binchen@cmm.chem.upenn.edu

Abstract: A combination of the aggregation-volume-bias and configurational-bias Monte Carlo algorithms and the umbrella sampling technique was applied to investigate two different binary vapor−liquid nucleation systems: water/ethanol and water/*n*-nonane. The simulations are able to reproduce the different nonideal nucleation behavior observed experimentally for these two systems, i.e., the mutual enhancement of nucleation rates for water/ethanol mixtures and the two-pathway nucleation for water/*n*-nonane mixtures. Structural analysis provides microscopic explanations for the observed nucleation behavior. In particular, the simulations show a large and size-dependent surface enrichment of ethanol in the water/ethanol droplets, which confirms the previous experimental interpretation for this system. The immiscibility observed even for small water/*n*-nonane clusters causes the two-pathway nucleation mechanism.

1. Introduction

Understanding binary nucleation is a first step toward the goal of explaining multicomponent nucleation that plays a critical role in many processes of atmospheric, environmental, and technological importance. In particular, binary mixtures consisting of water/alcohol,[1] water/alkane,[2] alcohol/alkane,[3] or short and long alcohols or alkanes[1a,4] have been the focus of many experimental investigations. Using sophisticated techniques, these experiments have provided data on the dependencies of binary nucleation rates on temperature, vapor pressure, and vapor composition. An important conclusion has emerged from the experimental studies, namely that the classical nucleation theory (CNT),[5] which is based on the so-called capillary approximation and has been satisfactorily applied to numerous one-component systems, is incapable of describing the nucleation behavior for many binary systems. For some nonideal mixtures, such as water/alcohol systems, CNT can even produce unphysical results.[1c,6] Using density functional theory (DFT),[6] it has been demonstrated that the deficiency of CNT arises from the fact that it fails to predict the differences in composition between the critical nucleus and the bulk liquid. This deficiency can lead to negative aggregation numbers for the surface active species and a prediction of decreasing nucleation rates with increasing partial pressure in violation of the nucleation theorem.[6] By incorporating an explicit description of the composition, the DFT approach is able to yield results that are thermodynamically consistent, but its solution obtained for a given model is only approximate, and sometimes the underlying model is too simple (e.g., a single Lennard-Jones interaction site) to allow direct comparison with experiments. In contrast, particle-based simulations are a more convenient tool since the solution should be exact for a given model and more complex force fields (e.g., articulated multisite models with separate terms representing first-order electrostatic and dispersive interactions) can be employed. However, previous simulation studies for binary nucleation have concentrated on simple model systems.[7] The structural insights obtained from the simulations can also be used to interpret the experimental data and to understand the shortcomings of CNT and other nucleation theories.

In this work, we report on a direct simulation study for two binary vapor−liquid nucleation systems: water/ethanol and

† University of Pennsylvania.
‡ University of Minnesota.

(1) (a) Zahoransky, R. A.; Peters, F. *J. Chem. Phys.* **1985**, *83*, 6425−6431. (b) Schmitt, J. L.; Whitten, J.; Adams, G. W.; Zalabsky, R. A. *J. Chem. Phys.* **1990**, *92*, 3693−3699. (c) Viisanen, Y.; Strey, R.; Laaksonen, A.; Kulmala, M. *J. Chem. Phys.* **1994**, *100*, 6062−6072. (d) Strey, R.; Viisanen, Y.; Wagner, P. E. *J. Chem. Phys.* **1995**, *103*, 4333−4345. (e) Wyslouzil, B. E.; Heath, C. H.; Cheung, J. L.; Wilemski, G. *J. Chem. Phys.* **2000**, *113*, 7317−7329.
(2) (a) Wagner, P. E.; Strey, R. *J. Phys. Chem. B* **2001**, *105*, 11656-11661. (b) Peeters, P.; Hrubý, J.; van Dongen, M. E. H. *J. Phys. Chem. B* **2001**, *105*, 11763−11771.
(3) Viisanen, Y.; Wagner, P. E.; Strey, R. *J. Chem. Phys.* **1998**, *108*, 4257−4266.
(4) (a) Strey, R.; Viisanen, Y. *J. Chem. Phys.* **1993**, *99*, 4693−4704. (b) Looijmans, K. N. H.; Luijten, C. C. M.; van Dongen, M. E. H. *J. Chem. Phys.* **1995**, *103*, 1714−1717.
(5) (a) Becker, R.; Döring, W. *Ann. Phys.* **1935**, *24*, 719−752. (b) Volmer, M. *Kinetik der Phasenbildung*; Steinkopff: Dresden, 1939. (c) Reiss, H. *J. Chem. Phys.* **1950**, *18*, 840−848. (d) Laaksonen, A.; Taalnquer, V.; Oxtoby, D. W. *Annu. Rev. Phys. Chem.* **1995**, *46*, 489−524.
(6) (a) Oxtoby, D. W.; Kashchiev, D. *J. Chem. Phys.* **1994**, *100*, 7665−7671. (b) Laaksonen, A.; Oxtoby, D. W. *J. Chem. Phys.* **1995**, *102*, 5803−5810. (c) Laaksonen, A.; *J. Chem. Phys.* **1997**, *106*, 7268−7274.
(7) (a) ten Wolde, P. R.; Frenkel, D. *J. Chem. Phys.* **1998**, *109*, 9919−9927. (b) Yoo, S.; Oh, K. J.; and Zeng, X. C. *J. Chem. Phys.* **2001**, *115*, 8518−8524;

water/*n*-nonane. These systems were selected because of their distinct nonideal nucleation behavior. The former exhibits a mutual nucleation enhancement,[1c] whereas the latter shows a two-pathway nucleation phenomenon.[2]

2. Simulation Details

The common task for simulations of nucleation behavior is to compute the nucleation free energy, $\Delta G(n_1, n_2)$, as function of cluster size and composition up to a size slightly larger than the critical nucleus or, equivalently, the cluster size distribution, $P(n_1, n_2) = \exp[-\Delta G(n_1, n_2)/k_BT]$. The simulation methodology employed here allows very efficient calculations of these equilibrium cluster properties using a combination of the aggregation-volume-bias Monte Carlo algorithm (AVBMC),[8] the configurational-bias Monte Carlo (CBMC) method,[9] and the umbrella sampling technique.[10] Compared to conventional simulation approaches, it has the following advantages.[11] First, efficient sampling of cluster growth and shrinkage can be achieved through AVBMC swap moves which target displacements that allow particles to move in or out of the aggregation region of the cluster. Compared to the unbiased translation move used in the conventional Metropolis Monte Carlo scheme,[12] the AVBMC swap move is able to balance energetic and entropic factors exhibited by monomers and clusters since both Boltzmann weight (energetic factor) and accessible volume (entropic factor) are taken into account in the transition probability of this move. Furthermore, the AVBMC scheme can be used in conjunction with CBMC growth strategies[9] to allow for efficient swaps of molecules with articulated structures. Once it is possible to expediently sample cluster growth and shrinkage, it becomes possible to single out one cluster from the entire system and turn a global problem into a local one by utilizing the equivalence between the cluster-size distribution of the entire system and the size distribution of the selected cluster. This significantly reduces the size of the system required for the simulation and also allows for a straightforward implementation of the umbrella sampling technique.[10] To improve the statistics, the umbrella potential can be chosen in a way that produces a nearly uniform size distribution for the selected cluster.[11]

For computational efficiency, the grand-canonical version of the nucleation algorithm[11] was used here in which the interactions between the selected cluster and the gas phase are neglected. As demonstrated previously,[11b] this is a valid approximation for the low-temperature, low-density cases of interest in this work. Since the water, alcohol, and alkane molecules are represented by multisite models, an energy-based cluster criterion was employed.[11b] A cluster is defined as a group of molecules of which every molecule has at least one neighbor in the group with an interaction energy below (i.e., more favorable) a threshold pair energy U_{cl}. A negative threshold energy close in magnitude to the simulation temperature was employed for all pairs of like or unlike molecules except for the water/*n*-nonane pair for which $U_{cl} = -30$ K was used.

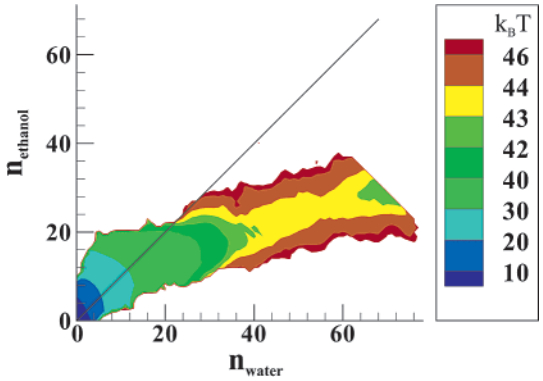

Figure 1. Contours of the two-dimensional nucleation free energy as a function of the number of water and ethanol molecules calculated from the simulation at $n_v^{water} = n_v^{ethanol} = 1.54 \times 10^{-7}$ Å^{-3}. The solid line denotes the average composition of the vapor phase.

In all calculations, ethanol and *n*-nonane were modeled by the TraPPE-UA force field.[13] The popular TIP4P model[14] was used for water. For comparison to experiments,[1c,2a] simulations were carried out at $T = 260$ K for the water/ethanol system and 230 K for the water/*n*-nonane system.

3. Simulation Results and Discussions

3. A. Water/Ethanol Mixtures. Plotted in Figure 1 are the contours of the two-dimensional nucleation free energy as a function of the number of water and ethanol molecules calculated from a simulation at $n_v^{water} = n_v^{ethanol} = 1.54 \times 10^{-7}$ Å^{-3} (the gas-phase activities are specified in terms of n_v, the number density of the ideal gas phase). The nucleation free energy profile for the water/ethanol mixture exhibits only one saddle point, thereby demonstrating that water and ethanol are "miscible" in the critical nucleus.

Figure 2 displays various combinations of onset activities for the vapor−liquid nucleation of the binary mixture of water and ethanol. These onset activities are normalized by the activities of neat water and neat ethanol vapors and correspond either to a constant nucleation rate of 10^7 cm^{-3} s^{-1} as measured experimentally[1c] or predicted by CNT[1c] or to a constant nucleation barrier height of 43 k_BT as calculated from the simulations. It should be noted that the nucleation rate is mainly determined by the nucleation barrier and that the preexponential factor depends only weakly on the vapor-phase activities.[5c] As is evident from this figure, both the experimental and simulation data show that nucleation of the water/ethanol mixture occurs at much lower activities than expected for an ideal mixture (for which the reduced onset activities simply fall on a straight line and sum to unity). These lower onset activities signal mutual enhancement of the nucleation for this mixture. By contrast, CNT predicts very different results. In particular, the use of the Gibbs−Thomson relations yields a "bulk" cluster composition that is very water rich[1c] or might even contain negative numbers of ethanol molecules.[6c] Water-rich clusters are characterized by larger surface tensions which in turn lead to lower nucleation

(8) (a) Chen, B.; Siepmann, J. I. *J. Phys. Chem. B* **2000**, *104*, 8725−8734. (b) Chen, B.; Siepmann, J. I. *J. Phys. Chem. B* **2001**, *105*, 11275−11282.
(9) (a) Siepmann, J. I.; Frenkel, D. *Mol. Phys.* **1992**, *75*, 59−70. (b) Frenkel, D.; Mooij, G. C. A. M.; Smit, B. *J. Phys.: Condens. Matter* **1992**, *4*, 3053−3076. (c) Martin, M. G.; Siepmann, J. I. *J. Phys. Chem. B* **1999**, *103*, 4508−4517.
(10) Torrie, G. M.; Valleau, J. P. *Chem. Phys. Lett.* **1974**, *28*, 578−581.
(11) (a) Chen, B.; Siepmann, J. I.; Oh, K. J.; Klein, M. L. *J. Chem. Phys.* **2001**, *115*, 10903−10913. (b) Chen, B.; Siepmann, J. I.; Oh, K. J.; Klein, M. L. *J. Chem. Phys.* **2002**, *116*, 4317−4329.
(12) Metropolis, N.; Rosenbluth, A. W.; Rosenbluth, M. N.; Teller, A. H.; Teller, E. *J. Chem. Phys.* **1953**, *21*, 1087−1092.
(13) (a) Martin, M. G.; Siepmann, J. I. *J. Phys. Chem. B* **1998**, *102*, 2569−2577. (b) Chen, B.; Potoff, J. J.; Siepmann, J. I. *J. Phys. Chem. B* **2001**,*105*, 3093−3104.
(14) Jorgensen, W. L.; Chandrasekhar, J.; Madura, J. D.; Impey, R. W.; Klein, M. L. *J. Chem. Phys.* **1983**, *79*, 926−935.

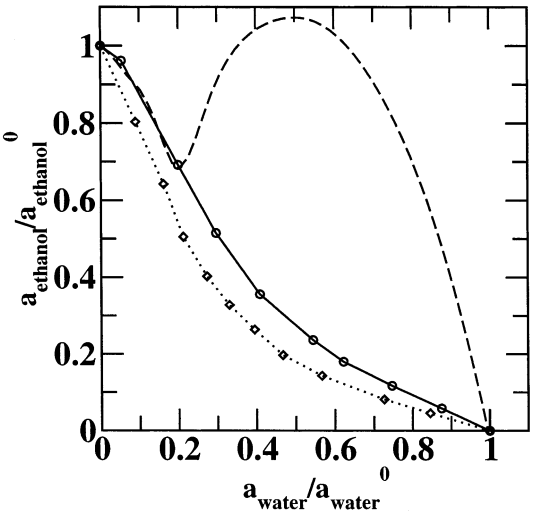

Figure 2. Reduced onset activities for binary nucleation of water/ethanol mixtures at 260 K. The experimental data (dotted line and diamonds) and the CNT predictions (dashed line)[1c] are for a constant nucleation rate of 10^7 cm^{-3} s^{-1}, whereas the simulation data (solid line and circles) are for a constant barrier height of 43 k_BT.

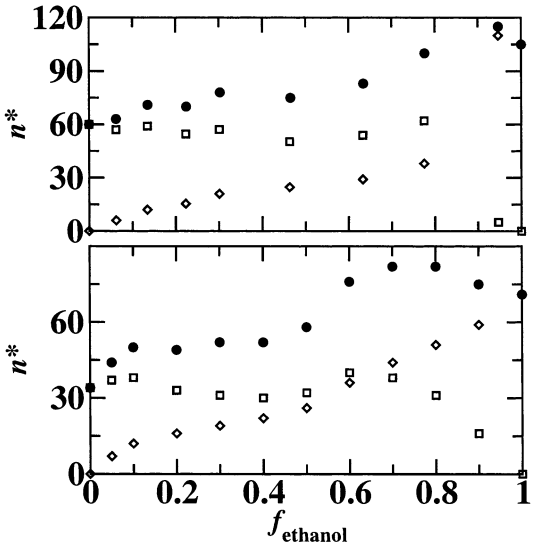

Figure 3. Molecular content of critical nuclei as function of normalized activity fraction of ethanol calculated from the simulation (top) and interpreted from the experimental data (bottom).[2c] The critical cluster size and the number of water and ethanol molecules in the nuclei are represented by circles, squares, and diamonds, respectively.

rates and higher critical onset activities. Much better agreement with experimental nucleation rates for the water/ethanol case can be achieved with the use of microscopic cluster models which explicitly account for differences in the interior and surface composition of the cluster.[1c,15]

The agreement between the experiments[1c] and the simulations also extends to the size and composition of the critical clusters (see Figure 3). Both indicate that the size and composition of the critical nuclei evolve in a nonlinear way as function of the normalized activity fraction, $f_{ethanol} = (a_{ethanol}/a_{ethanol}^0)/(a_{water}/a_{water}^0 + a_{ethanol}/a_{ethanol}^0)$[1c]. This nonideal behavior seems to arise mainly from the nearly constant number of water molecules in the critical cluster extending from pure water to $f_{ethanol} \approx 0.8$. It is noteworthy that both experiment and simulation indicate the unexpected existence of a slight maximum in the number of water molecules and the overall size of the critical nucleus at high $f_{ethanol}$ (of about 0.6 and 0.8, respectively). In contrast, the number of ethanol molecules increases in a more steady fashion with increasing normalized activity fraction, albeit the simulations show a substantial jump in the number of ethanol molecules for very high ethanol concentrations. An important outcome of the peculiar behavior of the number of water molecules with increasing $f_{ethanol}$ is that for water-rich vapors the critical nuclei are enriched in ethanol (compared to an ideal mixture), whereas the clusters are enriched with water for equimolar and ethanol-rich vapors (see also Figure 1). As discussed above, the failure of CNT can be traced back to the fact that CNT yields cluster compositions that are extremely water rich up to $f_{ethanol} \approx 0.8$.[1b,6]

Although the cluster sizes and compositions predicted by the simulations follow the same general behavior as those obtained in the experimental results, the sizes of the critical nuclei found in the simulations are about 50% larger, and the partial ethanol concentrations of the nuclei are lower in the simulations (with the exception of $f_{ethanol} = 0.947$). These discrepancies can be attributed to shortcomings of the nonpolarizable force fields used in this work. For example, they are known to slightly underpredict the air−water partitioning of primary alcohols[16a,b] and underestimate the mutual solubilities of water and 1-butanol.[16c]

Although CNT assumes that the critical cluster is uniform in composition, it is well-known that nonideal mixtures, such as water/ethanol, show substantial composition inhomogeneities near surfaces.[17] Allowing for different compositions of the surface layer and the interior of the critical nucleus and taking into account that the size of the critical nucleus increases with $f_{ethanol}$, the explicit cluster model also yields ethanol enrichment for water-rich vapors and vice versa.[1c] A snapshot of a critical nucleus immediately shows that surface enrichment is also an important feature for small clusters (see Figure 4). Analysis of radial density profiles of clusters with aggregation numbers close (±2 molecules) to the critical size allows further microscopic-level information to be obtained from the simulations (see Figure 5). With the exception of $f_{ethanol} = 0.947$, the radial density profiles appear to be remarkably similar and share many common features. First, as expected, there is a substantial surface excess of ethanol even for cases where the overall composition of the cluster is enriched in water. Second, the staggering of the ethanol oxygen and carbon densities indicates that the ethanol molecules are oriented with their polar moiety pointing toward the interior of the cluster and their alkyl tail toward the exterior (also evident at $f_{ethanol} = 0.947$). Third, up to $f_{ethanol} \approx 0.8$ the interior part ($r < 5$ Å) of the clusters is almost exclusively occupied by water, irrespective of the overall cluster composition. The water density begins to decrease around $r = 6$ Å for all three cases. In contrast, the peak heights and widths for the ethanol peaks increase with $f_{ethanol}$ (but it should be noted that droplet shape fluctuations contribute to the interfacial

(15) (a) Flageollet-Daniel, C.; Garnier, J. P.; Mirabel, P. *J. Chem. Phys.* **1983**, *78*, 2600−2606. (b) Laaksonen, A.; Kulmala, M. *J. Chem. Phys.* **1991**, *95*, 6745−6748. (c) Laaksonen, A. *J. Chem. Phys.* **1992**, *97*, 1983−1989.

(16) (a) Chen, B.; Siepmann, J. I. *J. Am. Chem. Soc.* **2000**, *122*, 6464−6467. (b) Chen, B.; Siepmann, J. I. *J. Phys. Chem. B* Submitted for publication. (c) Chen, B.; Siepmann, J. I.; Klein, M. L. *J. Am. Chem. Soc.* **2002**, *124*, 12232−12237.

(17) (a) Li, Z. X.; Lu, J. R.; Styrkas, D. A.; Thomas, R. K.; Rennie, A. R.; Penfold, J. *Mol. Phys.* **1993**, *80*, 925−939. (b) Matsumoto, M.; Nishi, N.; Furusawa, T.; Saita, M.; Takamuku, T.; Yamagami, M.; Yamaguchi, T. *B. Chem. Soc. JPN* **1995**, *68*, 1775−1783. (c) Raina, G.; Kulkarni, G. U.; Rao, C. N. R. *J. Phys. Chem. A* **2001**, *105*, 10204−10207.

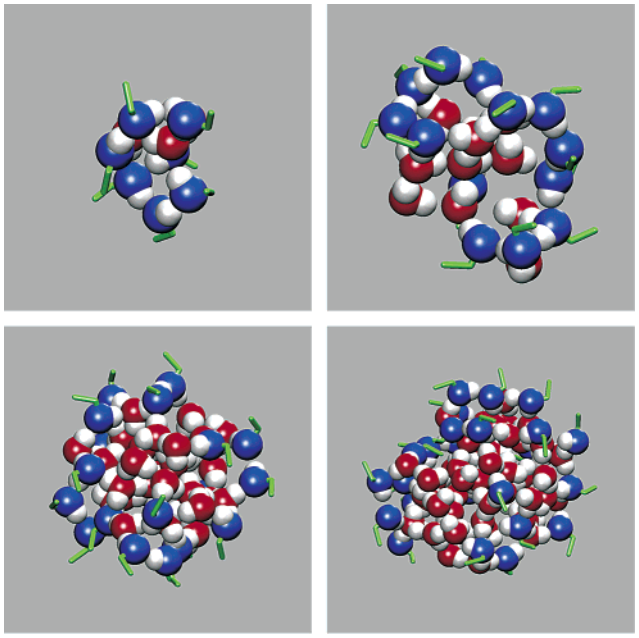

Figure 4. Snapshots of pre-critical clusters (containing a total of 10, 25, or 50 molecules) and the critical nucleus (75 molecules) for the water/ethanol mixture at $n_v^{water} = n_v^{ethanol} = 1.54 \times 10^{-7}$ Å^{-3}. Color notation: hydrogen (white), water oxygen (red), ethanol oxygen (blue), and alkyl tail (green stick).

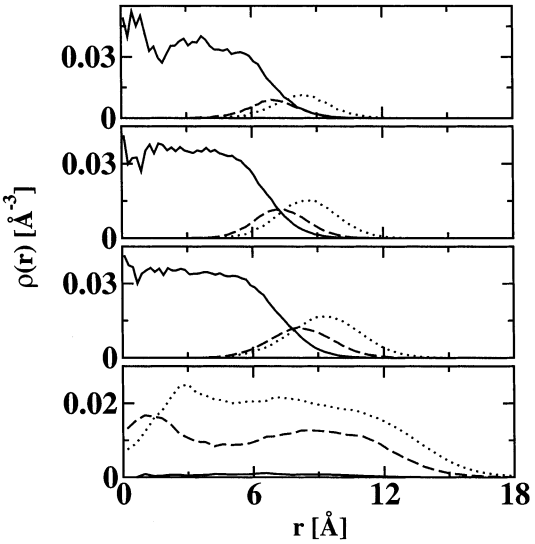

Figure 5. Radial number density profiles for the water oxygen atoms (solid lines), the ethanol oxygen atoms (dashed lines), and the ethanol carbon atoms (dotted lines) averaged over near-critical clusters taken from the simulations for normalized ethanol fractions of 0.224 (top), 0.465, 0.776, and 0.947 (bottom).

structure obtained from the radial density profiles). Thus, the picture that emerges from the simulations for $f_{ethanol} < 0.8$ is that of a well-preserved water core (viz. the relatively constant number of water molecules in the critical nucleus, see Figure 3) surrounded by a changing ethanol-rich corona. In contrast, the simulation at the highest ethanol concentration ($f_{ethanol} = 0.947$) demonstrates that the water core eventually vanishes and a relatively homogeneous distribution of water and ethanol is found in the cluster interior ($r < 10$ Å). This microscopic picture differs from the predictions of the explicit cluster model which yields substantial ethanol concentrations in the interior of the critical nucleus, e.g., $x_{ethanol}^{interior} \approx 0.2$ for $f_{ethanol} = 0.776$[1c]. Similarly, DFT calculations for Lennard-Jones mixtures with their unlike interactions modified to mimic water/alcohol mixtures, point toward a substantial concentration of the surface-active species in the interior of the critical nucleus.[6c] On the other hand, the structural results from this work are in general agreement with previous molecular dynamics simulations on small water/ethanol clusters with fixed composition (53 water and 7 ethanol molecules).[18] Nevertheless, there is agreement among the explicit cluster model, the DFT calculations, and the particle-based simulations that the compositions of the critical water/ethanol nuclei are inhomogeneous with substantial ethanol enrichment at the surfaces. The importance of organic surface layers for atmospheric nucleation and evolution has recently been emphasized.[19]

Regarding the mutual enhancement of nucleation rates for water/ethanol mixtures, the above structural findings provide a straightforward explanation, that is, enrichment of ethanol molecules lowers the surface tension and correspondingly the surface free energy. As shown by simulations for water/1-butanol mixtures using the same force fields as in the present work, the surface tension at the infinitely planar air−aqueous phase interface decreases by nearly 35% upon saturation with 1-butanol.[16c] Both water and alcohol benefit from the surface enrichment observed at the curved surface of the critical nuclei (this work) or at the infinitely planar surface.[16c] Hydrogen-bond analysis (using the criteria: $r_{OH} < 2.5$ Å and $-1 < \cos\theta_{OH\cdots O} < -0.4$[16c]) reveals significant increases of the average numbers of hydrogen bonds per molecule for the water/ethanol clusters. For water, it increases from 3.2 for the critical nucleus of pure water to 3.6 for the critical nucleus at $f_{ethanol} = 0.465$, whereas for ethanol, it increases from 2.0 for the pure ethanol cluster to 2.2 at $f_{ethanol} = 0.465$. The large increase of the number of hydrogen bonds for water is due to the decrease of the free hydrogen donors of surface water that are satisfied by the excess hydrogen-bond acceptors of ethanol. This, on the other hand, also leads to a gain of the number of hydrogen bonds for ethanol (note that an average number greater than two implies that ethanol molecules often accept more than one hydrogen bond). Furthermore, ethanol molecules preferentially act as hydrogen-bond donor for another ethanol molecule (see Figure 4), another sign for the microheterogeneity of the water/ethanol clusters.

Since the critical cluster dominates the nucleation rate, it is the focus of most experimental and theoretical investigations of nucleation behavior. However, the simulations described here sample the entire spectrum of cluster sizes from monomer to the critical nucleus. Thus, the simulations allow us to provide additional insight on the properties of pre-critical clusters. Snapshots of some pre-critical clusters (see Figure 4) give a first indication that the composition of the pre-critical clusters changes with cluster size. A similar picture emerges from the nucleation free energy surface shown in Figure 1, that the initial growth path is skewed toward ethanol-enriched clusters followed by a kink in the path that leads to water-enriched clusters before reaching the critical nucleus. A more quantitative picture can be obtained from calculations of the average cluster composition as a function of its size (see Figure 6). Irrespective of $f_{ethanol}$,

(18) Tarek, M.; Klein, M. L. *J. Phys. Chem. A* **1997**, *101*, 8639−8642.
(19) (a) Ellison, G. B.; Tuck, A. F.; Vaida, V. *J. Geophys. Res.* **1999**, *104*, 11633−11641. (b) Dobson, C. M.; Ellison, G. B.; Tuck, A. F.; Vaida, V. *Proc. Natl. Acad. Sci. U.S.A.* **2000**, *97*, 11864-11868. (c) Donaldson, D. J.; Tuck, A. F.; Vaida, V. *Orig. Life Evol. Biosphere* **2002**, *32*, 237−245.

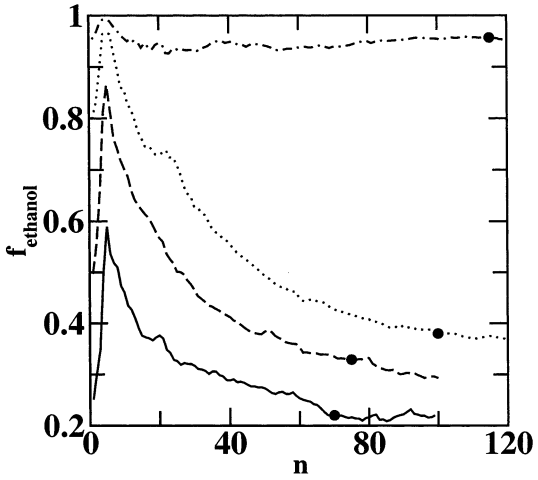

Figure 6. Average ethanol mole fractions versus cluster size. Results for nucleation at normalized ethanol fractions of 0.224, 0.465, 0.776, and 0.947 are depicted as solid, dashed, dotted, and dashed−dotted lines. The compositions of the critical nuclei are emphasized by filled circles.

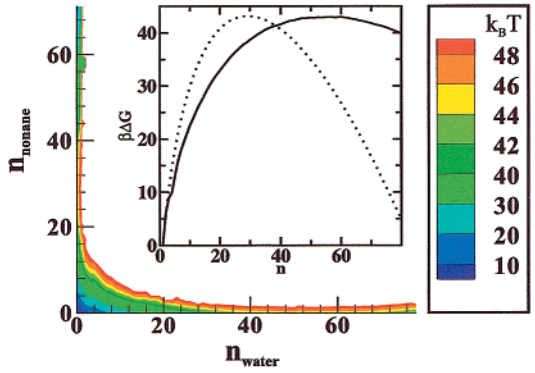

Figure 7. Contours of the two-dimensional nucleation free energy surface as a function of the number of water and *n*-nonane molecules calculated from the simulation at $n_v = 3.85 \times 10^{-8}$ Å^{-3} for water and $n_v = 1.31 \times 10^{-7}$ Å^{-3} for *n*-nonane. Shown in the inset are the one-dimensional nucleation free energy barriers for pure water (solid line) and pure *n*-nonane (dotted line) clusters.

all growing clusters show initial enrichment in ethanol with a sharp and pronounced maximum for clusters with a total aggregation number of 5. Thereafter, the ethanol concentration decreases and reaches a plateau around the critical cluster size.

3. B. Water/Nonane Mixtures. In recent experimental studies[2] it was found that the nucleation rates for supersaturated water/*n*-nonane vapors differ qualitatively from those of water/alcohol mixtures including those containing long-chain alcohols with bulk miscibility gap.[1d] These experimental results indicate two-pathway nucleation for the water/*n*-nonane mixtures.[2] While the simulations demonstrate that water and ethanol are "miscible" in the critical nucleus by showing one saddle point in the nucleation free energy profile (see Figure 1), water and *n*-nonane are immiscible in all combinations of gas-phase activities. Plotted in Figure 7 are the contours of the two-dimensional nucleation free energy as a function of the number of water and *n*-nonane molecules calculated from the simulation at $n_v = 3.85 \times 10^{-8}$ Å^{-3} for water and $n_v = 1.31 \times 10^{-7}$ Å^{-3} for *n*-nonane. It is evident that two saddle points located on the unary axes are present, each of which represents a separate nucleation path. The critical cluster sizes corresponding to the two saddle points differ markedly, i.e., the critical nucleus

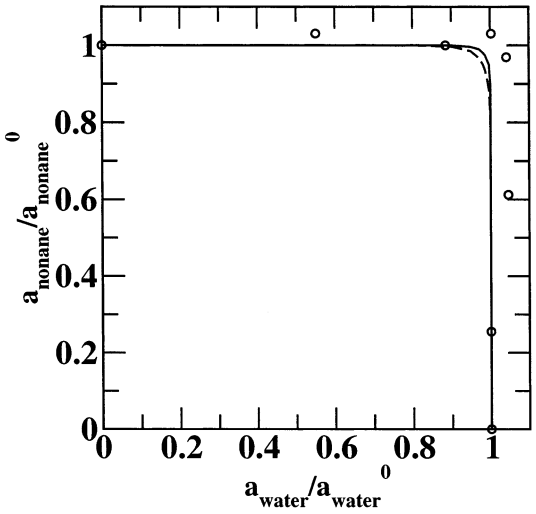

Figure 8. Reduced onset activities for binary nucleation of water/*n*-nonane mixtures at 230 K. The experimental data (circles) and the nucleation theorem predictions (dashed line)[2a,20] are for a constant nucleation rate of 10^7 cm^{-3} s^{-1}, whereas the simulation data (solid line) are for a combined constant barrier height of 43 k_BT.[21]

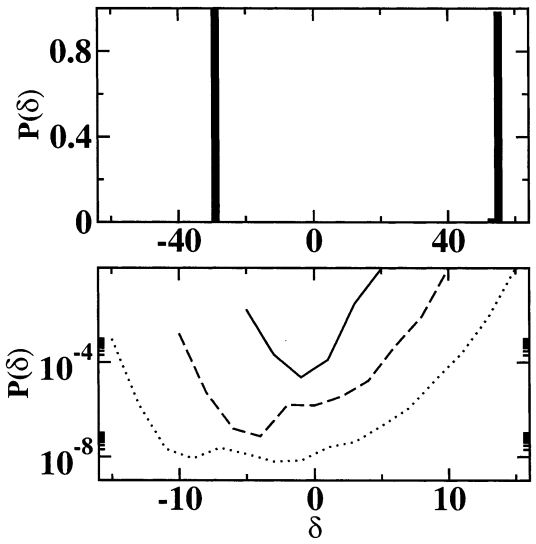

Figure 9. Distributions of the composition of the critical nuclei (top, shown as histograms and normalized separately for water- or nonane-rich droplets) and small pre-critical clusters (bottom, shown as lines and normalized for all nuclei with the same size) containing 5 (solid), 10 (dashed), and 15 (dotted) molecules as function of $\delta = n_{water} - n_{nonane}$ for nucleation of water/*n*-nonane vapors at $f_{nonane} = 0.5$.

observed for pure water contains about twice as many molecules as the critical nucleus for pure *n*-nonane.

In Figure 8, the critical onset activities for water/*n*-nonane mixtures obtained from experiment,[2a] the nucleation theorem for immiscible binary fluids,[20] and simulation are compared.

(20) Oxtoby, D. W.; Laaksonen, A.; *J. Chem. Phys.* **1995**, *102*, 6846−6850.
(21) For comparison to the experimental data and nucleation theorem predictions, the combined constant barrier height W^* is used, which is defined by the following: $\exp(-W^*/k_BT) = \exp(-W_1^*/k_BT) + \exp(-W_2^*/k_BT)$, where W_1^* and W_2^* are the barrier heights for the formation of the critical water- and nonane-rich droplets, respectively. The two-dimensional nucleation free energy surface obtained from the simulation at $n_{v0}^1 = 3.85 \times 10^{-8}$ Å^{-3} for water and $n_{v0}^2 = 1.31 \times 10^{-7}$ Å^{-3} for *n*-nonane was used to determine the free energy profiles at other sets of gas-phase activities as follows: $\Delta G_{n_v^1,n_v^2}(i_1, i_2) = \Delta G_{n_{v0}^1,n_{v0}^2}(i_1, i_2) + i_1 \times k_BT \ln(n_v^1/n_{v0}^1) + i_2 \times k_BT \ln(n_v^2/n_{v0}^2)$.[8a,22]
(22) Kusaka, I.; Wang, Z.-G.; Seinfeld, J. H. *J. Chem. Phys.* **1998**, *108*, 3416−3423.

Agreement is very satisfactory. The line of critical onset activities shows two straight parts which are connected by a small region with large curvature located at a normalized *n*-nonane fraction $f_{nonane} = 0.5$. Since the straight parts are nearly parallel to the axis system, it can be concluded that only one of the two separate nucleation pathways contributes to the overall nucleation behavior. The large curvature region corresponds to sudden changes in the composition of the critical nuclei.[20] The simulations allow us to unambiguously answer the question whether partial miscibility plays a role at the large curvature region or whether two kinds of pure critical nuclei are prevalent. Cluster composition distributions calculated for the critical nuclei and some pre-critical clusters at the large-curvature region are shown in Figure 9. These composition profiles show clearly that a mixture of pure critical nuclei is present at the large-curvature region. In addition, even very small pre-critical clusters show a distinct bimodal distribution at $f_{nonane} = 0.5$. This is also reflected in the nucleation free energy surface which shows a steep incline along a path of equimolar cluster composition (see Figure 7). The asymmetry in the probabilities for the small water- and nonane-rich clusters is caused by the differences in the steepness of the nucleation free energy pathways for either water- or nonane-rich clusters (see inset of Figure 7).

4. Conclusions

In conclusion, a combination of the aggregation-volume-bias Monte Carlo algorithm, the configurational-bias Monte Carlo algorithm, and the umbrella sampling technique was applied to investigate two different binary vapor−liquid nucleation systems: water/ethanol and water/*n*-nonane. These simulations have reproduced the different nucleation behavior found by the experiments for these two systems,[1,2] i.e., the mutual enhancement for nucleation of the water/ethanol vapors and the two-pathway nucleation of the water/*n*-nonane vapors. Structural analysis reveals that the formation of an ethanol-enriched surface region is responsible for the observed mutual enhancement and also the shortcomings of the CNT predictions for the water/ethanol system. For the water/*n*-nonane mixture, the microscopic immiscibility observed for the critical nuclei is the origin for the two-pathway nucleation mechanism.

Acknowledgment. We thank Ken Leopold, Bruce Garett, Greg Schenter, Shawn Kathmann, Veronica Vaida, Howard Reiss, and Kwang Jin Oh for many stimulating discussions. Financial support from the National Science Foundation CTS-0138393 (J.I.S.) and CHE-0205146 (M.L.K.) is gratefully acknowledged. Part of the computer resources were provided by the Minnesota Supercomputing Institute.

JA029006+